Uses of Abaqus/Standard in Failure Analysis

Matthew T. Kenner, P.E., John A. Wilkinson, P.E.,

Michael E. Stevenson, Ph.D., P.E., and Michael D. Hayes, Ph.D., P.E.

Engineering Systems Inc.
www.esi-website.com

Abstract: The capabilities of Abaqus as a design tool are widely known, but it is also a very effective tool for failure analysis and forensic engineering. This paper examines two case studies in which Abaqus/Standard was used to assist in determining the cause of failure. In the first instance, a motorcycle wheel was found severely deformed and broken after an accident. At issue was whether the wheel failure was caused by impact with the road after a "wheelie" or a concrete block after loss of control. Abaqus/Standard was used to simulate these loading conditions, which required contact and highly nonlinear material behavior. The results of these simulations were compared with the physical evidence and, combined with other evidence, demonstrated that the damage to the wheel was a result of the accident and not the cause. In the second instance, the top chord of a portal crane failed. Examination of the top chord found evidence of pre-existing cracks in multiple areas. Evidence also indicated some of the cracking had been repaired and subsequently re-initiated. Because of the beam's length, detailed crack analysis was not practical in a single model. Therefore, a submodeling approach was used to evaluate the localized effect of cracking. Various crack geometries were investigated with the fracture mechanics features of Abaqus/Standard to evaluate the residual strength of the damaged beam, the effectiveness of the repairs and the likely time history of cracking in the beam.

Keywords: Failure Analysis, Plasticity, Fatigue, Fracture Mechanics

1. Introduction

The finite element method has long been recognized as a valuable and capable design tool. While this is likely the most common use for Abaqus, its capabilities also make it a very effective tool for use in failure analysis and forensic engineering. In this role, Abaqus' strengths in simulating contact, material nonlinearities and fracture mechanics are quite useful, as these issues are very often important factors when trying to understand the cause of a structural failure. This paper examines two applications of Abaqus/Standard in failure analysis. In the first case, a motorcycle wheel was severely deformed and broken after an accident. The analysis of the wheel's failure required contact and material nonlinearity. In the second case, a beam used as the top chord of a portal crane failed. The beam had multiple fatigue cracks and Abaqus was used to evaluate the residual strength of the damaged beam for several different crack configurations.

2. Motorcycle Wheel Failure

2.1 Background

A rider was performing “wheelies” on a high-performance motorcycle when he lost control and crashed. The loss of control allegedly occurred near the conclusion of the “wheelie” when the front wheel was lowered to the ground. During the accident, the motorcycle tumbled and impacted a concrete block wall. Post-accident examination of the motorcycle’s front wheel showed it to be severely deformed and broken (see Figure 1). It was alleged that the front wheel failed as the motorcycle was lowered from the “wheelie” and this caused the loss of control, but the physical evidence suggested the front wheel directly and forcefully impacted the top corner of the wall as it tumbled.

Figure 1. Damaged motorcycle wheel.

2.2 Finite Element Models

In order to assist in resolving this question, Abaqus was used to compare the behavior of the wheel when loaded by a flat surface (i.e. coming down hard on the road) to that of the wheel when loaded by a 90° edge (i.e. the top corner of a concrete block wall). The two models are shown in Figure 2. While the load-deflection response of the wheel was of interest, the physical signatures of the wheel as a result of the different loads were also very important to assist in the interpretation of the physical evidence.

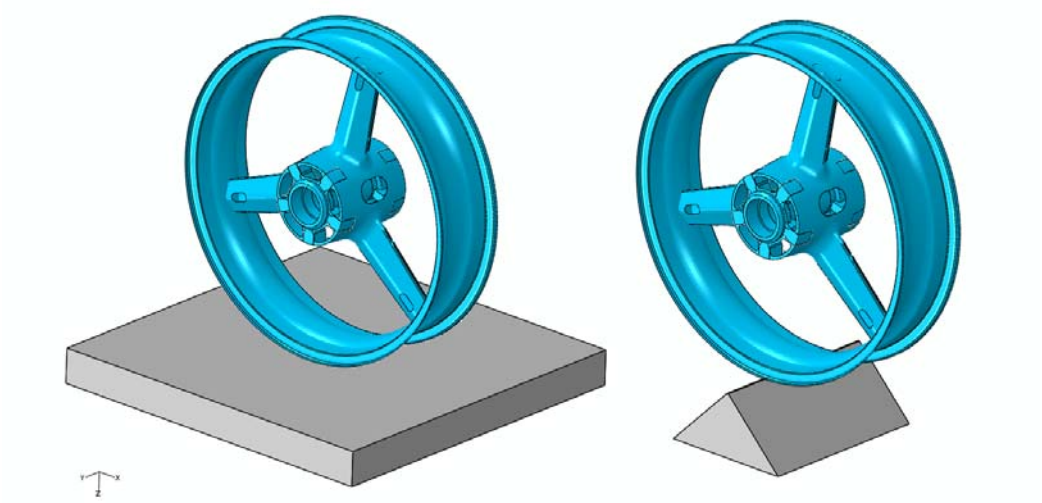

Figure 2. Model of the motorcycle wheel with a flat load block (left) and an edge load block (right).

While Abaqus is capable of performing a complete analysis of the tire/wheel interaction under dynamic loading, this level of complication and expense was not deemed necessary in this case. The analysis assumed that the tire would conform to the shape of the load block (flat or angled) and, therefore, did not have to be explicitly modeled – a reasonable assumption given that the tire unseats from the rim and deflates under the applied load. Also, because the exact dynamics of the impact to the wheel were not well defined, a static equivalent loading approach was used.

Exact material properties for the subject wheel were not available, but its chemical composition indicated the material was equivalent to A356.0 aluminum. The stress strain curve for A356.0-T6 was used (Brown, 2002), with a yield strength of 32,000 psi and an ultimate strength of 47,000 psi at 9% elongation. Multiple points were defined in the **`*Plastic`** card between the yield and ultimate strength to give reasonable fidelity in the post-yield material definition.

Most of the wheel casting was modeled with shell elements, but material thicknesses in the vicinity of the axle dictated the use of solid elements (a combination of tetrahedron and hexagonal elements joined by **`*TIE`** constraints). The transition between the solid and shell elements utilized **`*Shell to Solid Coupling`** to properly transfer forces and moments across the transition. Details of the mesh are shown in Figure 3. The loading blocks were modeled with analytical rigid surfaces. Display bodies were added to the model to simplify visualization of the rigid surfaces during post processing. Each model had roughly 500,000 degrees of freedom and the analyses were run on a PC with two processors.

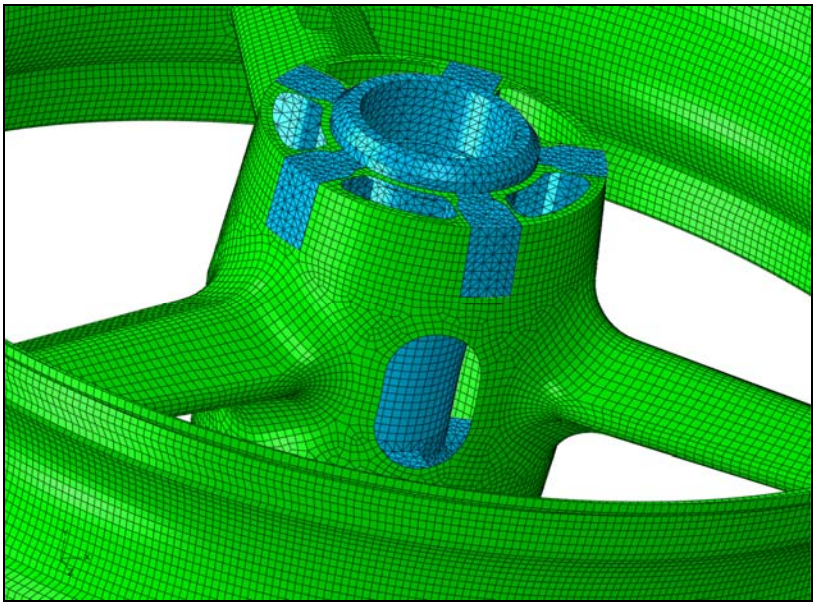

Figure 3. Details of the motorcycle wheel mesh.

A local cylindrical coordinate system was defined about the axle for the definition of boundary conditions. The bearing races were held fixed radially with the flats of the races held laterally. The wheel was prevented from spinning while contact was being established between the load blocks and the wheel, but once this contact was established this boundary condition was removed and the wheel was free to spin about its axle. Loading was accomplished with displacement control which is, of course, much more stable for nonlinear analysis. The load blocks were displaced into the wheel to the point where the brake rotor for the wheel would prevent further intrusion (roughly 2.5 inches).

2.3 Results and Discussion

The load-deflection curves for the analyses are shown in Figure 4. The von Mises stress results under full load block displacement are shown in Figure 5 and Figure 6. The load-deflection curves show that the maximum displacement requires more than twice the load for the flat load block. Also, the load curve flattens much more quickly with the edge load block. In both cases, the load on the wheel is severe; with stresses at, or near, the ultimate true stress of 51,000 psi. This is to be expected, given the significant impingement by the load block and the fact that the subject wheel fractured in numerous locations (Figure 1). In both cases, the area of loading experiences some of the highest stresses. Additional areas of high stress are the intersections of the spokes with the hub and the rim. All these areas were fractured in the subject wheel. Note, though, that the results from the flat load block show high stresses in areas that did not fracture on the subject wheel, indicating that contact with a flat surface may not have been the most probable scenario.

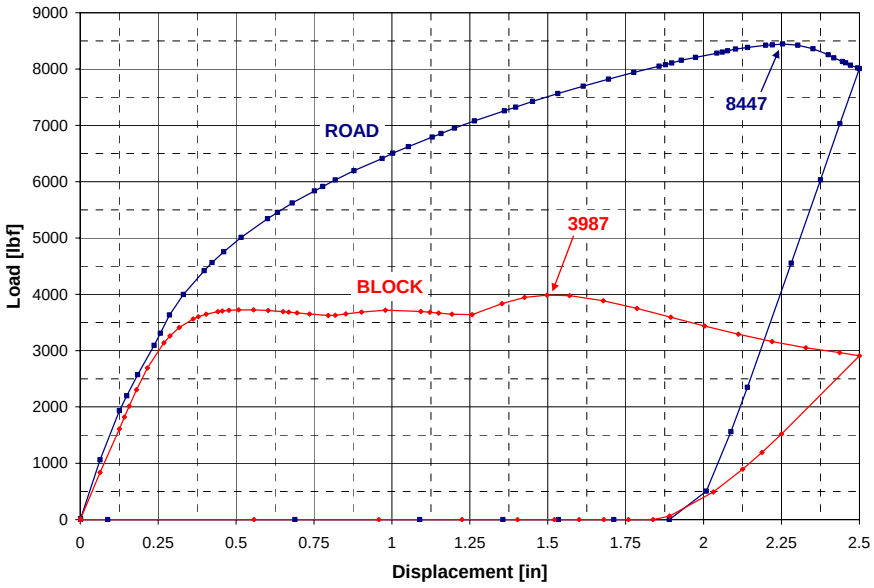

Figure 4. Motorcycle wheel load-deflection curves.

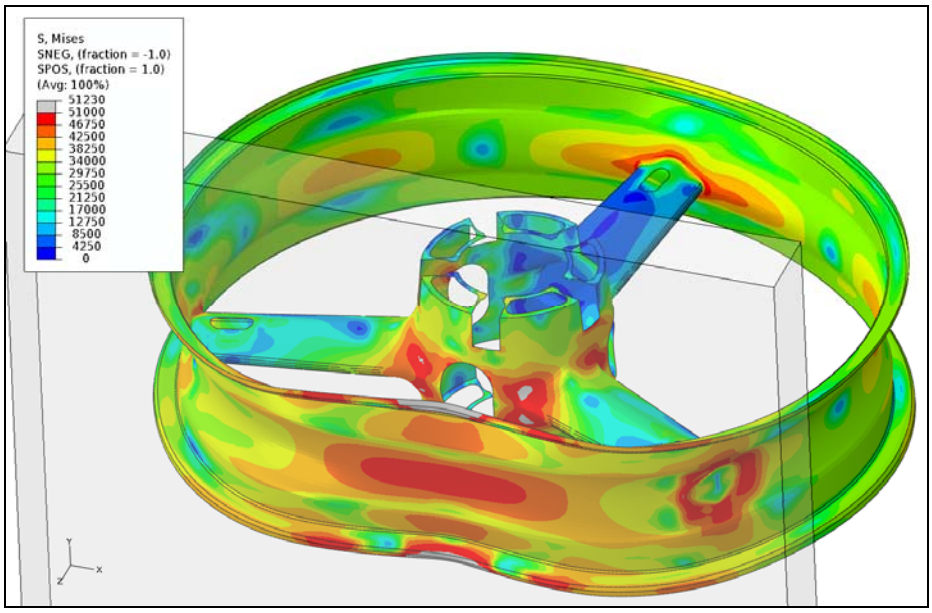

Figure 5. Flat load block von Mises stress results at full displacement (psi).

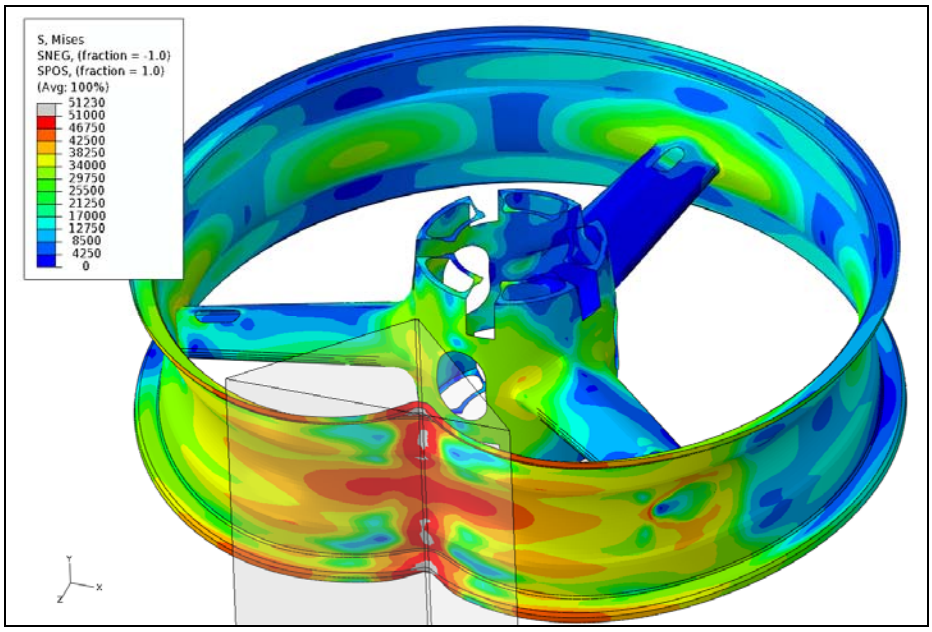

Figure 6. Edge load block von Mises stress results at full displacement (psi).

The deformed shapes of the wheel after unloading are shown in Figure 7. It can be seen that the residual shape in the area of the edge load block retains a severe bend after the block is removed. This is not the case with the flat load block. Comparing the analysis results to the subject wheel's rim fracture (Figure 8) clearly shows the similarity between the edge load block analysis and the subject wheel. Close examination of the wheel fracture in this region also shows that the edge of the rim was flattened in the vicinity of the fracture. This phenomenon was shown to occur under loading from the edge load block but not the flat load block.

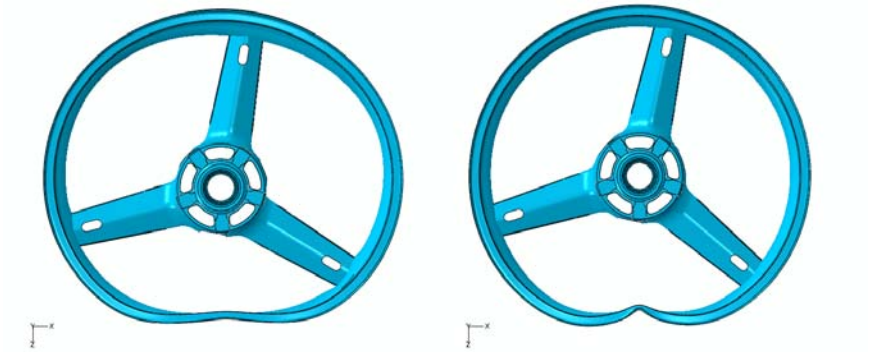

Figure 7. Deformed shape after unloading of the flat load block (left) and the edge load block (right).

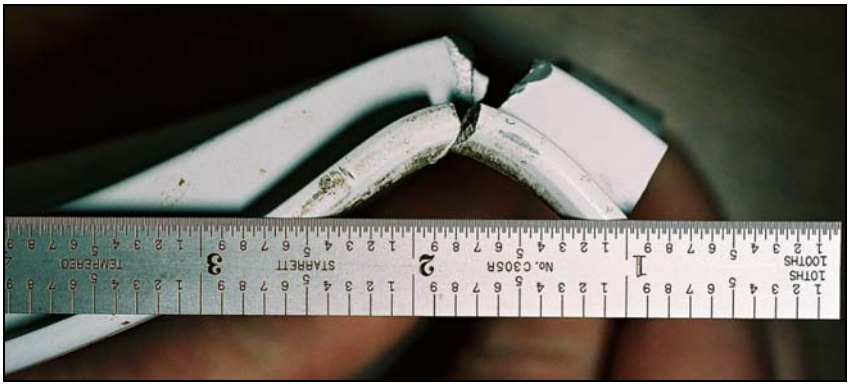

Figure 8. Details of the wheel fracture in the area of the load block.

It is clear from the analyses that the signatures on the failed wheel more closely match the edge load block analysis. Of course, the edge load block closely approximates the top of the concrete wall which suffered significant damage as a result of the accident. Additionally, the results show the edge load generates stresses near failure at roughly half the load required by a flat load block. This becomes significant when considering the load to fail the wheel is generated only by the inertia of a motorcycle and rider that weighs roughly 600 lbs and, in the wheelie scenario, a portion of that weight is reacted at the rear wheel. In the final analysis, considering the factors discussed above, as well as other aspects of the investigation that are not discussed here, it was determined that the front wheel of the motorcycle did not cause the loss of control.

3. Portal Crane Failure

3.1 Background

The subject crane was a portal crane used at a lumber yard. Portal cranes come in many configurations, but this particular crane used a structural arrangement similar to the generic portal crane shown in Figure 9.

Figure 9. General arrangement of the subject portal crane.

During the subject accident, the portal crane failed as the cab, hoist and load approached the extreme end of its travel on the outboard side of the larger vertical supporting member, as indicated in Figure 9.

The main structural member of the portal crane was a long space frame with a triangular cross-section. It used one built-up beam as the top chord and two built-up beams, separated by intermediate and diagonal bracing, as the bottom chord. The operator's cab and hoist assembly was suspended from, and travelled along, the bottom chord of the space frame. A network of diagonal pipes was used to connect the top and bottom chords of the truss to create the final geometry of the space frame. Figure 10 illustrates the general arrangement of the space frame and the three beams used as chord members.

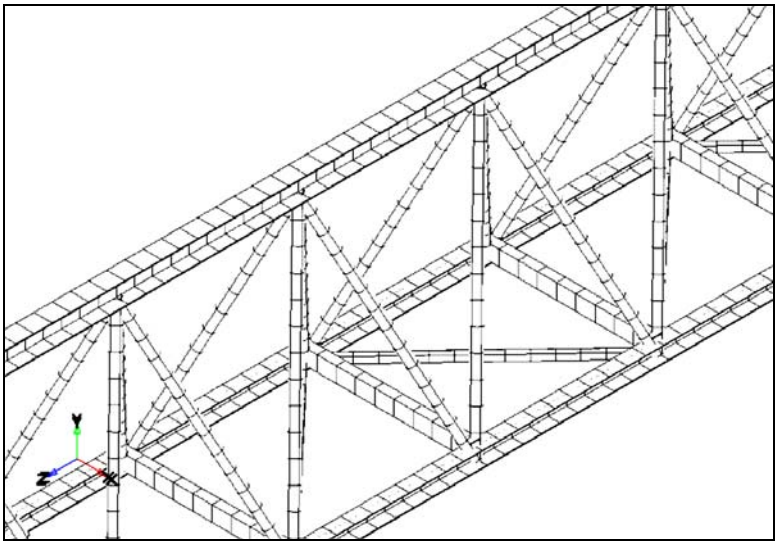

Figure 10. General arrangement of the space frame.

The accident occurred due to a sudden fracture of the top chord at a joint immediately outboard of the larger vertical supporting structure, as shown in Figure 11. The longitudinal chords of the truss were custom-fabricated ("built-up") sections that became thinner toward the ends of the space frame (lower bending moments call for smaller moments of inertia). The design accomplished this by varying the web and flange thicknesses, but also by reinforcing the webs of the beams with thick plates. In the section where the primary failure occurred, one such transition in section size and properties occurred immediately inboard of one of the joints where the diagonal tube members were welded to the bottom flange of the top chord. In addition, this change in section was located immediately outboard of the larger vertical support structure.

This structural arrangement created a complex stress state that resulted in high local stresses under normal loading when the cab assembly, including the hoist and its load, traveled to the extreme outboard end of the space frame (i.e., outboard of the larger vertical supporting structure). The overhanging load (a maximum of 32,000 lbf) when the cab and hoist were in the extreme outboard

position created a bending moment which induced tensile stresses in the top chord of the space frame that were then amplified by the joint detail.

Further exacerbating the situation, all of the joints were stiffened by welding in four vertical L-shaped plates between the flanges of the beam, effectively forming a box-like structure between the two flanges, immediately above the location where the four tubes were welded to the bottom flange. This box structure prevented proper inspection of the various connections during service. A further complicating factor in this area was the addition of weld repairs during the crane's service, but prior to the final failure. The truss failed at the change in section in the subject joint, immediately inboard of the box-like structure, as shown by the hatched plane in Figure 13. One concern was whether the weld repairs may have contributed to this failure.

3.2 Finite Element Models

3.2.1 Global Model

To determine the forces and moments acting at the location of interest, ESI created a global 3D model of the main truss structure, as shown in a representational form in Figure 11.

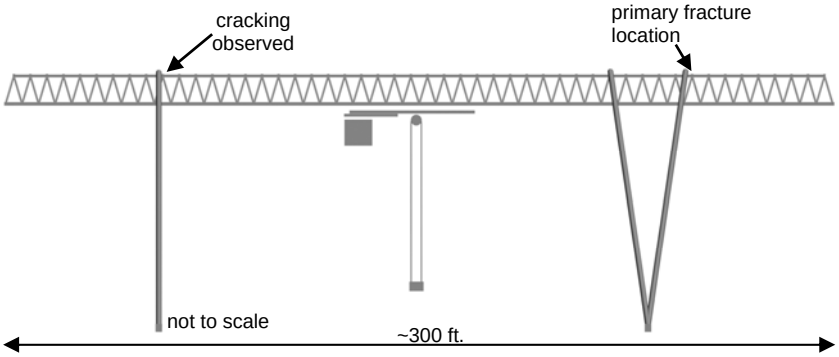

Figure 11. Side elevation of the subject portal crane.

The space frame members were modeled using beam elements. Various loading scenarios were examined during the investigation, but in the end a single critical load case was identified as being the most likely cause of the failure: normal operation with the cab, hoist and load located at the extreme end of the space frame, outboard of the larger vertical support, as shown in Figure 12. This location results in a maximum 32,000 lbf downward vertical load being applied at the right-hand end of the space frame.

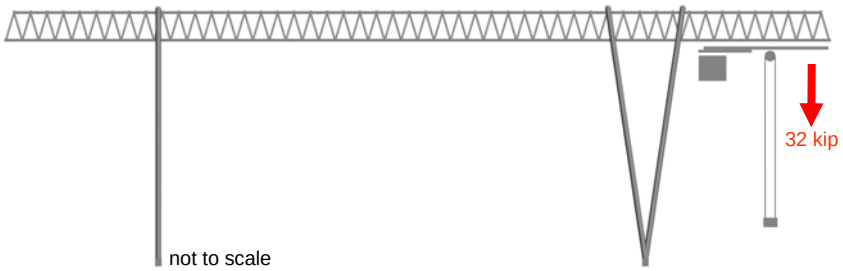

Figure 12. Vertical load case.

This downward vertical load produces tension in the top chord at the failure location, which is consistent with the fatigue cracking observed at the failure location, and the final sudden failure that occurred at the time of the accident. Therefore, the nodal displacements acting on either side of the failure location for this load case were extracted from the 3D global model and used to drive a refined local model. This detailed model was used to more precisely determine the local stresses that may have caused the fatigue cracking that led to the final failure.

3.2.2 Local Models

As noted above, a solid element local model was defined and analyzed using Abaqus/Standard to assess the detailed stress distribution at and near the fracture plane. The local model was assigned boundary conditions using nodal displacements taken from the global model at the location of the "cut" edges in the local model, as shown in Figure 13.

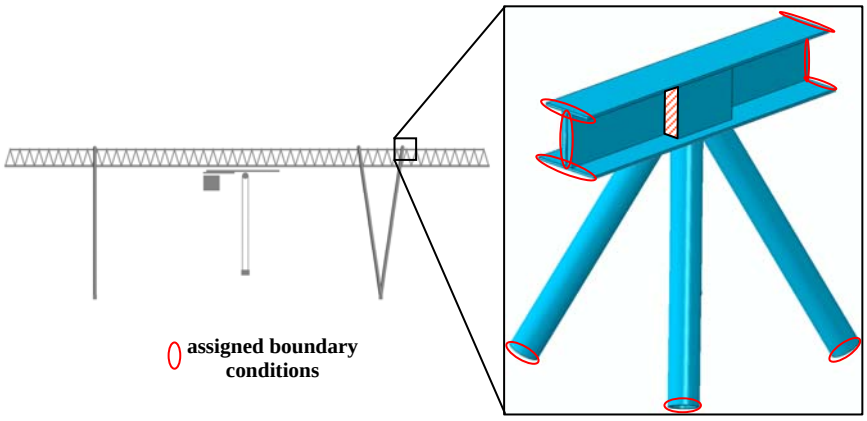

Figure 13. Top chord at the failure location - local model.

3.3 Results and Discussion

Figure 14 presents the overall longitudinal (S33) stress results for an un-cracked version of the detailed local model. Note the thick plates welded to the beam on either side of the web, inboard of the box structure. Figure 15 presents two S33 stress plots of the local model at, and outboard, of the fracture plane (components removed for clarity). Note the four "hot spots" located where the welds tying the thick web reinforcement plates to the box structure and the flanges join up. Three welds run into one discrete corner at each of these four locations. The maximum longitudinal stress at these hot spots was found to be 32 ksi for a nominal 1g vertical load. As a result, these high local stresses were determined to be sufficient to initiate the fatigue cracks that were observed at all four locations after the accident.

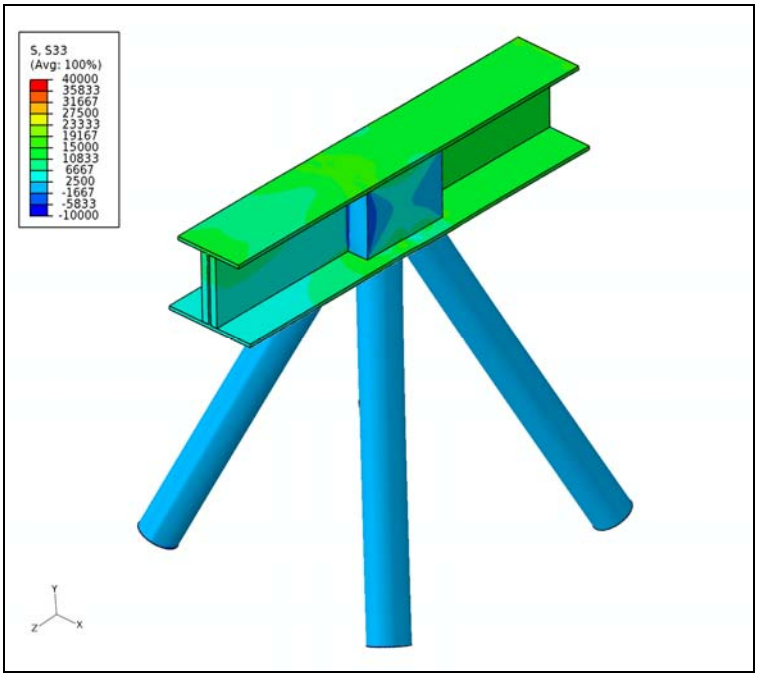

Figure 14. Local model – right tip load (F_Y = -32,000 lbf) – S33 (psi).

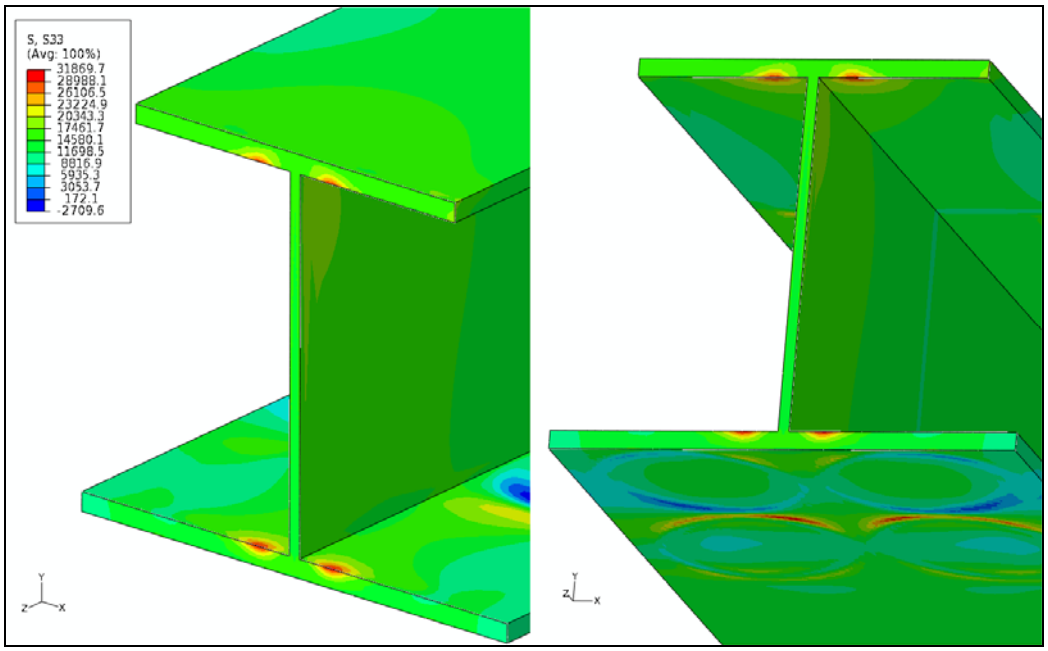

Figure 15. Local model – right tip load (F_Y = -32,000 lbf) – fracture plane – S33 (psi).

After establishing the local stresses for an un-cracked top chord, ESI investigated stress intensities for four different pre-existing crack cases that various parties contended may have existed at the time of final failure. These crack cases consisted of various combinations of the through-cracks and surface cracks. For each individual crack, a detailed mesh containing the crack geometry was inserted into the detailed local model and joined to the surrounding material using **`*TIE`** constraints. Stress intensities at the crack tips were calculated using the Contour Integral approach built into Abaqus, without including focused meshes along the crack fronts (Wilkinson, 2004).

The results for two of the crack cases are presented below in Figure 16 and Figure 17. Figure 16 illustrates a case with three through-cracks and one surface crack, accounting for all four hot spots. Figure 17 presents a case in which the through-crack in the lower left of Figure 16 has been repaired, while the other cracks remain.

The fatigue cracks in these figures can be identified by the low stresses on the crack surfaces (blue contours). Also, note that the location and magnitude of the maximum stress intensity for each crack is identified in both figures.

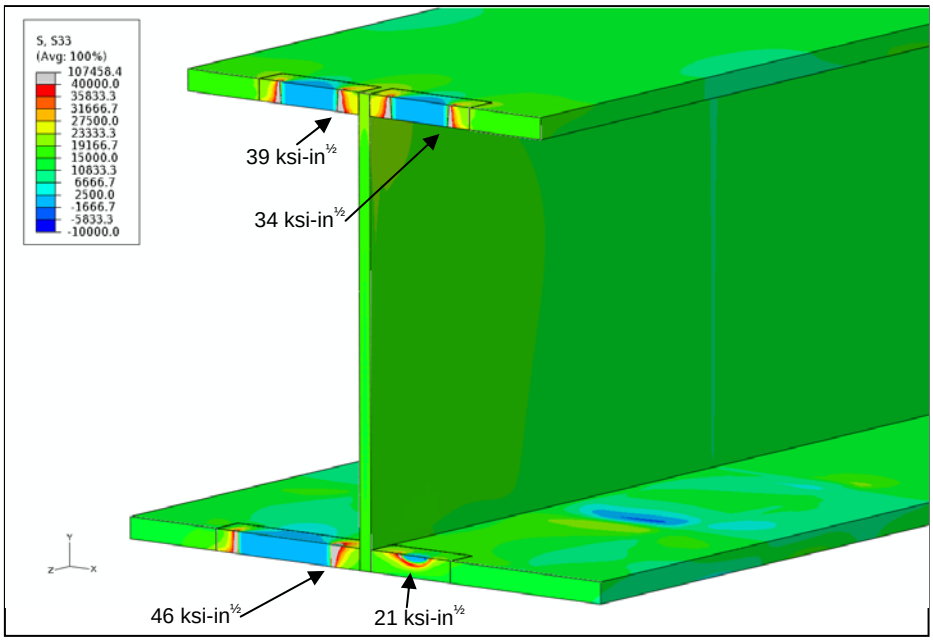

Figure 16. Stress intensities – crack configuration A – S33 (psi).

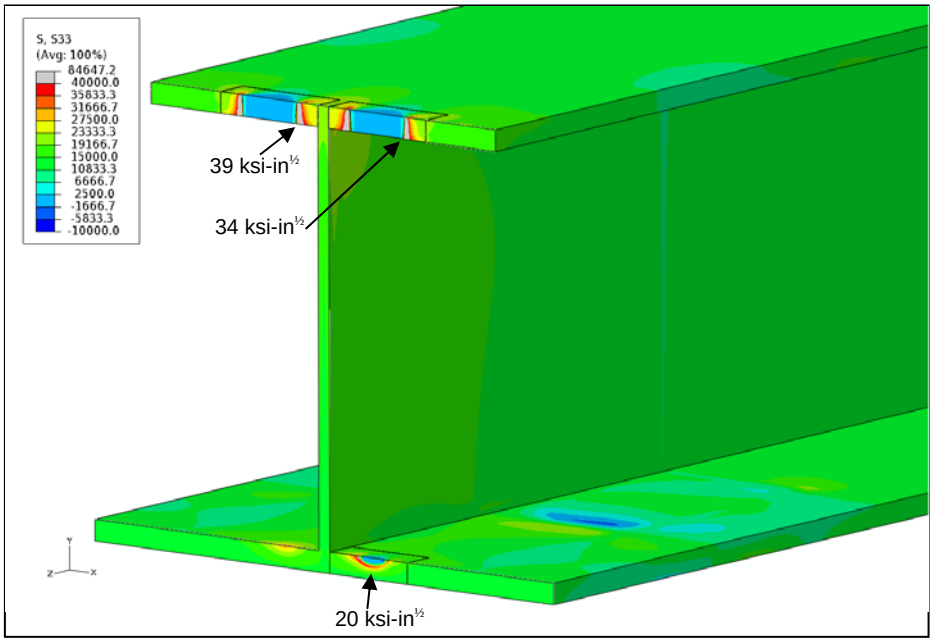

Figure 17. Stress intensities – crack configuration B – S33 (psi).

Examination of the stress intensities obtained for the four crack configurations for the 1G vertical load case, including the two shown above, clearly indicated that fatigue crack propagation could reasonably be expected on both the top and bottom flanges under both loading/crack configurations. In fact, there was little to no change in the crack tip stress intensities in the cases presented. Both scenarios exhibited crack tip stress intensities well above the threshold levels for structural steel. Evaluation of these scenarios allowed for the exclusion of the possibility that an inappropriate weld repair after fatigue crack growth had already initiated was largely responsible for the ultimate collapse.

4. Conclusions

The finite element method is not only an effective design tool, but is also a valuable tool for use in failure analysis. The capabilities of Abaqus/Standard were used to good advantage in the analysis of a motorcycle wheel, which fractured during an accident. The finite element analysis showed the signatures of the failed wheel most likely resulted from contact with a concrete block. In the case of the portal crane, Abaqus/Standard, in concert with a comprehensive failure analysis and a metallurgical investigation, helped determine the most likely pre-cracked condition for the top chord of the space frame at the time of the accident.

5. References

1. Abaqus/Standard Version 6.6 Analysis User's Manual, 2006.
2. Brown, W.F. and L.R. Hill, "Aerospace Structural Metals Handbook," CINDAS/USAF CRDA Handbooks Operation, vol. 3, 36th edition, 2002.
3. Wilkinson, J.A., M.T. Kenner and E.W. Holmes, "Stress Intensities for a Thumbnail-Shaped Surface Crack in a Solid Cylinder," Conference Proceedings, Abaqus Users' Conference, 2004.